Thin film LaYbO3 capacitive structures grown by pulsed laser deposition

Vasta, G.; Jackson, T.J.; Feteira, A.; Woodward, D.I.; Walker, D.; Thomas, P.A.

DOI:
10.1016/j.tsf.2012.12.006

Document Version
Publisher's PDF, also known as Version of record

Citation for published version (Harvard):
Vasta, G, Jackson, TJ, Feteira, A, Woodward, DI, Walker, D & Thomas, PA 2013, 'Thin film $LaYbO_3$ capacitive structures grown by pulsed laser deposition', *Thin Solid Films*, vol. 527, pp. 81-86.
https://doi.org/10.1016/j.tsf.2012.12.006

Thin Solid Films 527 (2013) 81–86

Contents lists available at SciVerse ScienceDirect

Thin Solid Films

journal homepage: www.elsevier.com/locate/tsf

Thin film $LaYbO_3$ capacitive structures grown by pulsed laser deposition

Giuseppe Vasta [a,*], Antonio Feteira [b,1], David I. Woodward [c,2], David Walker [c,3], Pam A. Thomas [c,4], Timothy J. Jackson [a,5]

[a] The University of Birmingham, School of Electrical Electronic and Computer Engineering, 52 Pritchatts Road, Edgbaston, Birmingham B15 2TT, UK
[b] The University of Birmingham, School of Chemistry, Edgbaston, Birmingham B15 2TT, UK
[c] University of Warwick, Department of Physics, Coventry, CV4 7AL, UK

ARTICLE INFO

Article history:
Received 8 May 2012
Received in revised form 6 December 2012
Accepted 7 December 2012
Available online 19 December 2012

Keywords:
Lanthanide ytterbium oxide
Thin films
Dielectric properties
Crystal structure
Pulsed laser deposition

ABSTRACT

The crystal structure and the dielectric properties of $LaYbO_3$ films grown by pulsed laser deposition and integrated in $SrRuO_3/LaYbO_3/SrRuO_3$ capacitive structures are reported. Two different fabrication procedures are assessed. When the $SrRuO_3/LaYbO_3/SrRuO_3$ stack is grown in-situ, the relative permittivity of the $LaYbO_3$ is 35. When instead the lower $SrRuO_3$ electrode layer is patterned by contact photolithography and argon ion milling, prior to the deposition of the $LaYbO_3$, the relative permittivity of the $LaYbO_3$ is 55. In this case, post-growth annealing brings the relative permittivity towards that of the film grown in-situ. In both cases the relative permittivity is higher than the value measured in bulk material. This is attributed to the permittivity being highest along the orthorhombic c-axis. The annealing procedure produced a recrystallization of the $LaYbO_3$ and of the $SrRuO_3$.

1. Introduction

Recently, interlanthanide perovskites (such as $LaLuO_3$) have been investigated as potential candidates to replace SiO_2 as high-k gate dielectrics, because of their high relative permittivity ε_r, low leakage current, and suitability for deposition by several techniques such as pulsed laser deposition (PLD), molecular beam deposition and atomic layer deposition [1,2]. These films are also expected to operate well at frequencies ranging from a few Hz to GHz in particular with low dielectric losses. The crystal structure and dielectric properties of $LaYbO_3$ and $LaLuO_3$ ceramics have been recently investigated. Relative permittivities of 26 and 22 were determined at room temperature for $LaYbO_3$ and $LaLuO_3$ respectively [3,4]. Schubert et al. [5] deposited epitaxial thin films of $LaLuO_3$ by PLD. In this communication, we report the structure and electrical properties of $SrRuO_3/LaYbO_3/SrRuO_3$ thin film capacitors also fabricated by PLD.

2. Experimental procedure

2.1. Target preparation

$LaYbO_3$ ceramic targets were prepared by the conventional mixed oxide route. High-purity grade La_2O_3 and Yb_2O_3 powders (both 99.99% purity, Aldrich Chemical Co., Milwaukee, WI) were weighed in a 1:1 molar ratio and intimately mixed by ball milling for 20 h, using yttria-stabilized zirconia balls. The dried slurry was calcined in air at 1200 °C and then at 1400 °C for periods of 15 h. To enhance sinterability, the calcined powder was re-milled by ball milling for 20 h. The finely milled calcined powder was uniaxially pressed into a 15 mm diameter pellet using an applied pressure of ~190 MPa. This green compact was subsequently fired for 4 h in air at 1600 °C, using a controlled heating–cooling rate of 5 °C/min.

The phase purity and crystallinity of the sintered $LaYbO_3$ target were determined by X-ray diffraction using a Siemens Model D5000 diffractometer operating with $CuK\alpha_1$ radiation, $\lambda = 1.54059$ Å. A step size of 0.02° and a scan rate of 2°/min were used for the scans.

2.2. Fabrication of the $SrRuO_3/LaYbO_3/SrRuO_3$ capacitors

$SrRuO_3/LaYbO_3/SrRuO_3$ thin film tri-layers were grown on (001)-oriented $SrTiO_3$ substrates by PLD using a KrF excimer laser with a wavelength of 248 nm. A 4 Hz repetition rate was used with the laser beam focused to a spot size of 2.4 mm^2 on the target, providing a fluence of 3.4 J/cm^2. The distance between the $SrTiO_3$ substrate and the target material was set to 5.7 cm. All the films were grown at a

Abbreviations: PLD, pulsed laser deposition.

* Corresponding author. Tel.: +44 1214144348.
E-mail addresses: pipvast@yahoo.it (G. Vasta), a.feteira@bham.ac.uk (A. Feteira), d.i.woodward@warwick.ac.uk (D.I. Woodward), d.walker.2@warwick.ac.uk (D. Walker), P.A.Thomas@warwick.ac.uk (P.A. Thomas), T.J.Jackson@bham.ac.uk (T.J. Jackson).
[1] Tel.: +44 1214147813.
[2] Tel.: +44 2476151782.
[3] Tel.: +44 2476151299.
[4] Tel.: +44 2476523354.
[5] Tel.: +44 1214144291.

0040-6090/$ – see front matter © 2012 Elsevier B.V. All rights reserved.
http://dx.doi.org/10.1016/j.tsf.2012.12.006

temperature of 780 °C and in flowing oxygen. The pressure was 40 Pa for the $SrRuO_3$ and 40 or 0.40 Pa for the $LaYbO_3$. The deposition rates were 0.012 nm/pulse for $SrRuO_3$ and 0.017 nm/pulse for $LaYbO_3$, corresponding to average growth rates of 0.048 nm s^{-1} and 0.068 nm s^{-1} respectively.

After the thin film deposition the samples were cooled in 90 kPa of static oxygen, with dwells of 15 min at 600 °C and of 30 min at 450 °C during cooling to fully oxygenate the deposited films. This is in agreement with the fabrication procedure employed for other perovskite oxides grown by PLD technique [6–8].

The thin films were patterned by contact photolithography and argon ion beam milling, using a Karl Suss mask aligner and an Oxford Applied Research IM150 ion milling system. S1813 photoresist was used to protect the regions of the films which constitute the capacitive structure.

Two different procedures were employed for the fabrication of the $SrRuO_3/LaYbO_3/SrRuO_3$ capacitors. In the first procedure, the $SrRuO_3$ bottom electrode layer was first grown by PLD and then patterned ex-situ using photolithography and ion-beam milling. Subsequently the $SrRuO_3/LaYbO_3$ bi-layer was grown. Further ex-situ patterning was performed, again using photolithography followed by ion-beam milling. The $SrRuO_3$ top electrode was defined and windows were opened through the $LaYbO_3$ film to enable electrical contact to the $SrRuO_3$ bottom electrode. A sketch of the side view of a device obtained with the first fabrication procedure is shown in Fig. 1a. In the second fabrication procedure, the $SrRuO_3/LaYbO_3/SrRuO_3$ tri-layer was grown in-situ. The top electrode geometry was then defined and then windows were opened through the $LaYbO_3$ to contact the bottom electrode. A sketch of the side view of a device obtained with the second fabrication procedure is shown in Fig. 1b. In both cases the following film thicknesses have been employed for the fabrication of the capacitive structures: 150 nm for the $SrRuO_3$ bottom electrode, 580 nm for the $LaYbO_3$ dielectric layer and 100 nm for the $SrRuO_3$ top electrode.

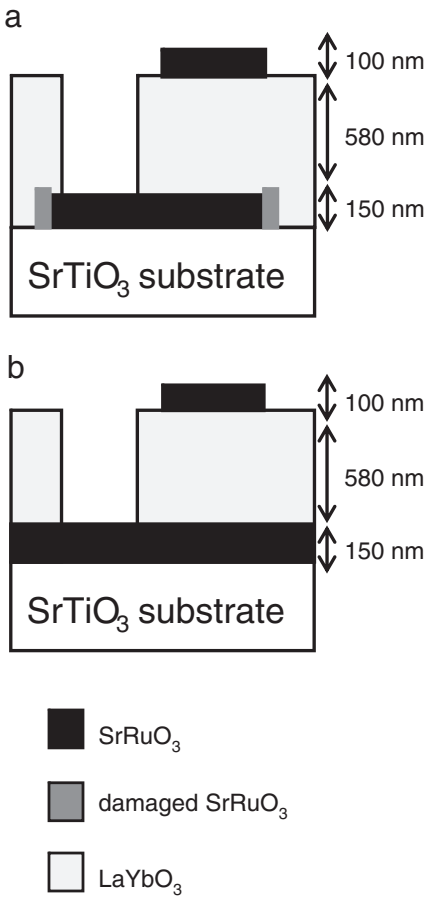

Fig. 1. a) Side view schematic of a $SrRuO_3/LaYbO_3/SrRuO_3$ parallel plate capacitor where both the $SrRuO_3$ top and bottom electrodes were patterned by contact photolithography and argon ion beam milling. In the figure the area of the bottom electrode damaged by the argon ion beam milling is indicated by the dark gray shading. b) Side view schematic of a $SrRuO_3/LaYbO_3/SrRuO_3$ parallel plate capacitor where the thin film tri-layer was grown in-situ.

The difference between the two procedures is in the patterning of the bottom electrode layer.

Post-growth annealing totaling 22 h duration at 500 °C in 10^5 Pa of flowing oxygen was performed on the capacitive structures fabricated with the first procedure.

2.3. Structural and dielectric investigation of the capacitive structures

$LaYbO_3$ has an orthorhombic crystal structure. In powder diffraction studies, $LaYbO_3$ was described by the space group *Pnma* with a = 6.033 Å, b = 8.432 Å and c = 5.843 Å [4]. In this paper it is described by space group *Pbnm* with lattice parameters of a = 5.843 Å, b = 6.033 Å and c = 8.432 Å. This choice of space group is consistent with the work of Schubert et al. on $LaLuO_3$ thin films prepared on $SrRuO_3/SrTiO_3$ [5]. It is also consistent with a convention for perovskite thin films where the longest axis is denoted the c-axis and is often desired to be parallel to the substrate normal. The matrix for converting Miller indices from the pseudo-cubic space group Pm-3m to the orthorhombic Pbnm space group is given by Eq. (1):

$$\begin{bmatrix} h \\ k \\ l \end{bmatrix}_o = \begin{bmatrix} 1 & 1 & 0 \\ 1 & -1 & 0 \\ 0 & 0 & 2 \end{bmatrix} \begin{bmatrix} h \\ k \\ l \end{bmatrix}_c . \quad (1)$$

When indexing planes in this paper, the subscript "c" is to denote cubic symmetry and the subscript "o" is used for the orthorhombic symmetry.

High-resolution X-ray diffraction was performed using a Panalytical X'Pert Pro diffractometer equipped with a hybrid Ge monochromator giving $CuK\alpha_1$ radiation. Substrates were mounted on a glass slide with the film layer facing upwards and the diffractometer was aligned to the $(001)_c$ peak of the substrate. $SrTiO_3$ has a simple cubic perovskite structure with lattice constant of 3.905 Å [9]. Two types of scan were performed. The first was a $2\theta-\omega$ scan through the substrate $(00l)_c$ peaks in order to collect all the film peaks corresponding to planes parallel to the substrate $(00l)_c$ planes. The second was a scan of the section of reciprocal space around the $(001)_c$ $SrTiO_3$ peak, in order to collect the corresponding $(002)_o$ $LaYbO_3$ and the $(001)_c$ $SrRuO_3$ peaks from the thin layers. $SrRuO_3$ is often considered as a pseudocubic perovskite with lattice constant of 3.93 Å when grown on $SrTiO_3$ [10] so its diffraction peaks are labeled with the subscript "c" like those of the substrate.

Impedance measurements of the fabricated structures were performed using an Agilent 4294A precision impedance analyzer with a source voltage amplitude of 1 V over the frequency range of 50 Hz–50 kHz.

3. Results and discussion

3.1. X-ray diffraction analysis

All of the results presented in this Section 3.1 correspond to films grown using the first fabrication procedure (i.e. with the ex-situ patterning of the $SrRuO_3$ bottom electrode layer).

Fig. 2 shows the results of $2\theta-\omega$ scans performed on two $SrRuO_3/LaYbO_3/SrRuO_3$ capacitive structures. Fig. 2a shows the $2\theta-\omega$ scan of an as-grown sample which did not undergo the post-growth annealing treatment. Fig. 2b shows the $2\theta-\omega$ scan of a similar sample after 22 h post-growth annealing. The peaks with their labels together with the assigned reflections are summarized in Table 1. The peaks labeled

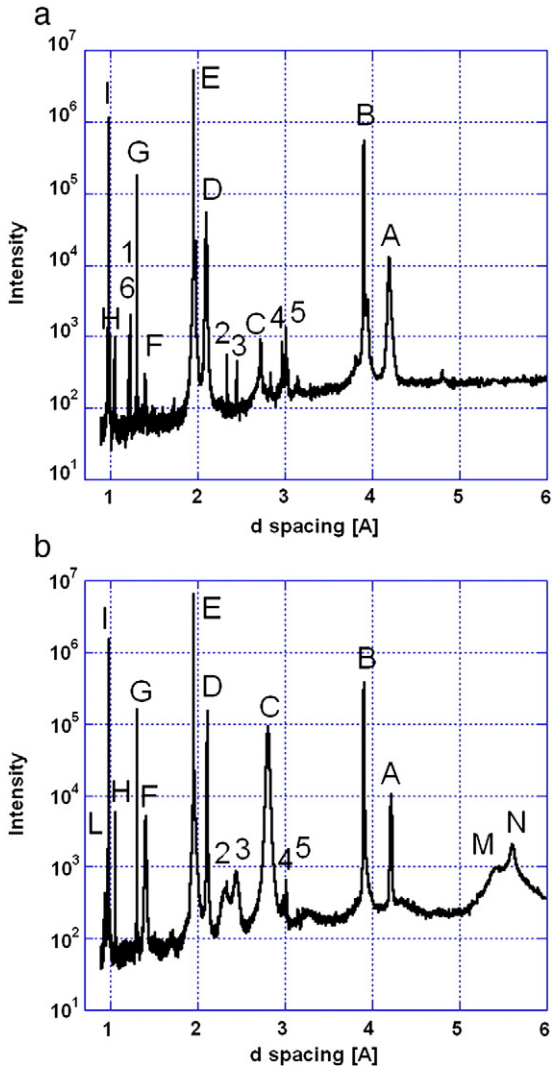

Fig. 2. a) $2\theta-\omega$ scan of a $SrRuO_3$(100 nm)/$LaYbO_3$(300 nm)/$SrRuO_3$(150 nm) capacitive structure grown on an $(001)_c$ $SrTiO_3$ substrate. This sample was not annealed. b) $2\theta-\omega$ scan of a $SrRuO_3$(100 nm)/$LaYbO_3$(580 nm)/$SrRuO_3$(150 nm) capacitive structure grown on an $(001)_c$-oriented $SrTiO_3$ substrate. This sample underwent the 22 hour post-growth annealing at 500 °C in 10^5 Pa of oxygen.

with the letters A–I are present in both the annealed and in the as-grown sample. Of the peaks labeled with the numbers, peaks 1 and 6 are only present in the as-grown sample. Peaks arising from the $SrTiO_3$ $\{00l\}_c$ and $LaYbO_3$ $\{00l\}_o$ planes are visible in both scans.

The labels B and E mark the $(001)_c$ and the $(002)_c$ planes respectively of $SrTiO_3$ and $SrRuO_3$. In the as-grown sample both the $SrTiO_3$ and $SrRuO_3$ peaks are visible at B and E. In the annealed sample there are single peaks at B and E, in other words the $SrRuO_3$ peaks are too close to the substrate peaks to be resolved. The peaks at G and I correspond to the $(003)_c$ and $(004)_c$ $SrTiO_3$ planes.

Peaks A, D and H correspond to the $(002)_o$, $(004)_o$ and $(008)_o$ $LaYbO_3$ reflections. Peak F is the $(006)_o$ $LaYbO_3$ reflection and may include a contribution from the $(220)_c$ $SrRuO_3$ reflection. The relative intensities of the $LaYbO_3$ film peaks are consistent with the intensities of the same reflections measured on bulk $LaYbO_3$ [4].

In well aligned growth the $2\theta-\omega$ scans should consist of only peaks corresponding to both the cubic and orthorhombic $\{00l\}$ planes oriented parallel to the substrate surface, however peaks C and F originating from the $(110)_c$ and possibly the $(220)_c$ $SrRuO_3$ planes appear in the scans of both the annealed and the as-grown samples.

From the data it appears that during the patterning of the $SrRuO_3$ bottom electrode, the edges of the electrode area may have been damaged by the argon ion milling necessary to define the electrode geometry. The $(110)_c$ and $(220)_c$ peaks (peaks C and F) are believed to originate from recrystallization of the $SrRuO_3$ at the edges of the electrode during the heating of the sample for the deposition of the subsequent $LaYbO_3$ and $SrRuO_3$ layers. The higher intensity or narrowing of film peaks A, C, D, F and H after the post-growth annealing, as shown in Fig. 2b, is consistent with further changes in crystal structure during annealing [11].

Table 1
Peak labels, interplanar spacings d, 2θ values and corresponding indexing of the planes from the $2\theta-\omega$ scans in Fig. 2. The two samples have been labeled as GV01D and GV02D; GV01D is the sample which was not annealed (see Fig. 2a) while the sample GV02D underwent the 22 hour post-growth annealing at 500 °C in $100*10^3$ Pa of oxygen (see Fig. 2b). The symbol "–" means: the peaks were not present. Peaks L, M and N could not be assigned without ambiguity and are discussed in the text.

Peak label	d spacing [Å]		2θ [degree]		Reflection
	GV01D	GV02D	GV01D	GV02D	
N	–	5.5604	–	15.800	
M	–	5.4488	–	16.253	
A	4.1917	4.2189	21.177	21.039	$(002)_o$ LYO
B	3.905	3.905	22.753	22.753	$(001)_c$ STO + $(001)_c$ SRO
5	3.0127	3.0127	29.626	29.626	$(020)_o$ LYO
4	2.9683	2.9759	30.079	30.001	$(112)_o$ LYO
C	2.7203	2.8037	32.896	31.891	$(110)_c$ SRO
3	2.4481	2.4405	36.677	36.796	$(022)_o$ LYO
2	2.3380	2.3369	38.470	38.489	$(202)_o$ LYO
D	2.098	2.1099	43.078	42.822	$(004)_o$ LYO
E	1.9526	1.9526	46.466	46.466	$(002)_c$ STO + $(002)_c$ SRO
F	1.3983	1.4034	66.851	66.575	$(006)_o$ LYO + $(220)_c$ SRO
G	1.3016	1.3016	72.563	72.563	$(003)_c$ STO
1	1.2245	–	77.959	–	$(044)_o$ LYO
6	1.200	–	79.830	–	$(404)_o$ LYO
H	1.0496	1.0548	94.424	93.814	$(008)_o$ LYO
I	0.9760	0.97631	104.210	104.170	$(004)_c$ STO
L	–	0.93469	–	110.99	

Peaks 1–6 in Table 1 originate from $LaYbO_3$ planes which do not belong to the $\{00l\}_o$ family. Their relative intensities are also consistent with the measurements performed on the $LaYbO_3$ target [4]. These peaks arise from misaligned regions present in the $LaYbO_3$ film and are more prevalent in the as-grown sample (Fig. 2a). The presence of these regions might be due to a different orientation of the $LaYbO_3$ on the edges of the recrystallized $SrRuO_3$. It should be noted that peaks 4 and 5, $(112)_o$ and $(020)_o$ reflections respectively, were the most intense peaks measured in diffraction from the $LaYbO_3$ target; only a small amount of $(112)_o$- or $(020)_o$-oriented $LaYbO_3$ is required in the film to produce peaks having a significant intensity.

During the post-growth annealing, recrystallization also takes place in the $LaYbO_3$. After annealing, the $(044)_o$ and $(404)_o$ peaks (1 and 6 in Table 1) are not seen (Fig. 2b), indicating that regions of the film with these orientations become reoriented during annealing. In $LaLuO_3$ films, $[00l]_o$-oriented domains were seen to become dominant over $[hh0]_o$-oriented domains [5]; this was understood from the recognition that in $LaLuO_3$ the basal-plane diagonal is almost equal to the c-axis lattice parameter. In $LaYbO_3$, the lattice parameters corresponding to the $(044)_o$ and $(404)_o$ peaks are close to 1/7th of the c-axis lattice parameter, suggesting that these planes can easily reorient themselves. In contrast, recrystallisation did not lead to disappearance of peaks 2, 3, 4 and 5 in the $LaYbO_3$ films considered here, which may be a result of the fact that these do not display a close match to the c-axis lattice parameter.

After annealing, three extra peaks labeled L, M and N in Fig. 2(b) appeared which further substantiate the analysis. The peaks M and N are particularly broad. Since the assignments for all three cannot be made without ambiguity they are not included in Table 1. Peaks L and N may be associated with recrystallized $SrRuO_3$ that is not epitaxial with the substrate; peak N with a $(100)_o$ or $(001)_o$ reflection and

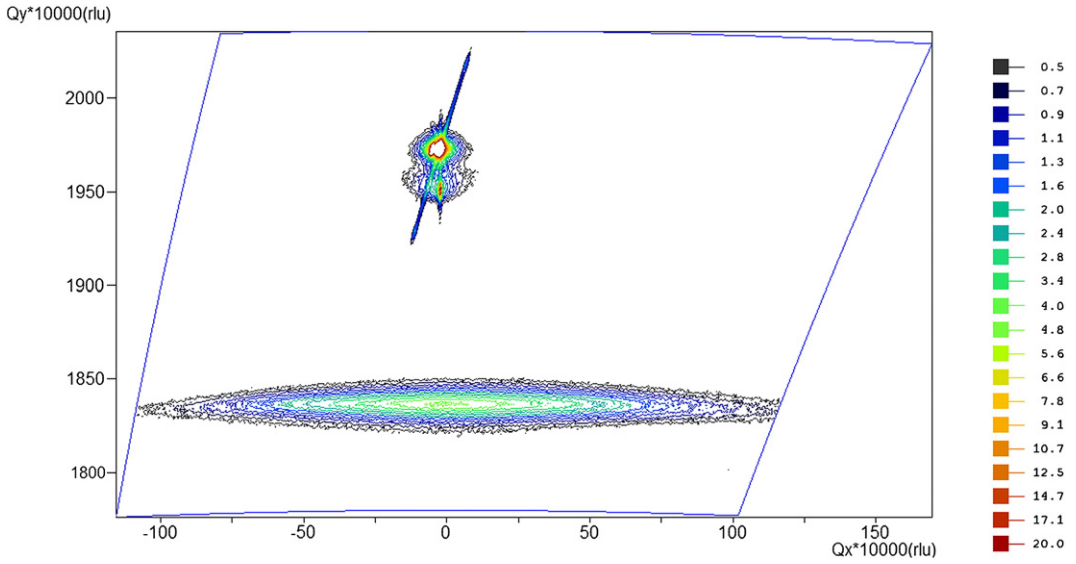

Fig. 3. Reciprocal space map of the region around the $SrTiO_3$ $(001)_c$ peak for the $SrRuO_3$(100 nm)/$LaYbO_3$(300 nm)/$SrRuO_3$(150 nm) capacitive structure which did not undergo the post-growth annealing treatment. The most intense peak is the $SrTiO_3$ $(001)_c$ peak. The broad peak at the bottom is the $LaYbO_3$ $(002)_o$ peak. Q_x and Q_y are defined in the following way: $Q_x = 1/2(\text{Cos}\ \omega - \text{Cos}\ (2\theta - \omega))$ and $Q_y = 1/2(\text{Sin}\ \omega + \text{Sin}\ (2\theta - \omega))$.

peak L with the $(164)_o$ or $(600)_o$ reflection. Peak M may be associated with a strain-induced phase transition producing a $1/2(120)_o$ $LaYbO_3$ reflection.

The orientation of the $SrRuO_3/LaYbO_3/SrRuO_3$ trilayers was studied with the help of reciprocal space maps. Fig. 3 shows a reciprocal space map of the region around the $SrTiO_3$ $(001)_c$ peak for the as-grown sample (this is the same sample whose $2\theta - \omega$ scan is reported in Fig. 2a). The most intense peak corresponds to the $(001)_c$ planes of the $SrTiO_3$ substrate. The broad peak at the bottom of the scan corresponds to the $LaYbO_3$ $(002)_o$ planes. The breadth of the peak indicates that, across the extent of the film, there is a significant mosaic spread in the $LaYbO_3$ layer. The center of this broad peak appears to be at the same position on the Q_x-axis as the $SrTiO_3$ peak, indicating that the $LaYbO_3$ $(002)_o$ planes are aligned with the $(001)_c$ planes of the substrate.

The data in Fig. 4 represent the reciprocal space map of a $SrRuO_3/LaYbO_3/SrRuO_3$ trilayer after the post-growth annealing treatment (this is the same sample whose $2\theta - \omega$ scan is reported in Fig. 2b). The $LaYbO_3$ $(002)_o$ peak, while still broad, is significantly less broad than in Fig. 3, showing that the annealing procedure has reduced the mosaic spread. To the right of the substrate peak there is a strong $SrRuO_3$ $(001)_c$ peak which shows that this $SrRuO_3$ is relaxed and slightly mis-aligned with respect to the substrate. To the right of this peak is a trail of intensity, indicating a population of $SrRuO_3$ which is less well aligned, possibly arising from the recrystallization which takes place at the edges of the bottom electrode geometry. The thin line passing through the $SrTiO_3$ peak (Figs. 3 and 4) is a truncation rod, a phenomenon arising from the diffractometer geometry and unconnected with the structure of the sample.

It can be concluded that the post-growth annealing re-crystallizes some mis-oriented regions in the $LaYbO_3$ film and repairs damage to the bottom electrode caused by the ion-milling necessary to define its geometry.

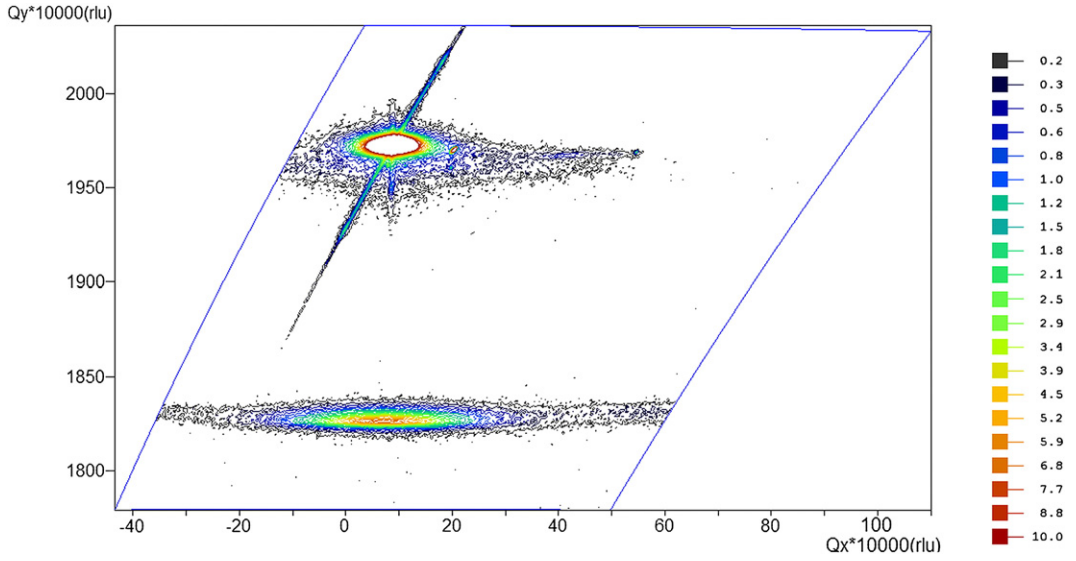

Fig. 4. Reciprocal space map of the region around the $SrTiO_3$ $(001)_c$ peak for the $SrRuO_3$(100 nm)/$LaYbO_3$(580 nm)/$SrRuO_3$(150 nm) trilayer after the post-growth annealing procedure. The most intense peak is the $SrTiO_3$ $(001)_c$ peak. The peak at the bottom is the $LaYbO_3$ $(002)_o$ peak. Q_x and Q_y are defined in the following way: $Q_x = 1/2(\text{Cos}\ \omega - \text{Cos}\ (2\theta - \omega))$ and $Q_y = 1/2(\text{Sin}\ \omega + \text{Sin}\ (2\theta - \omega))$.

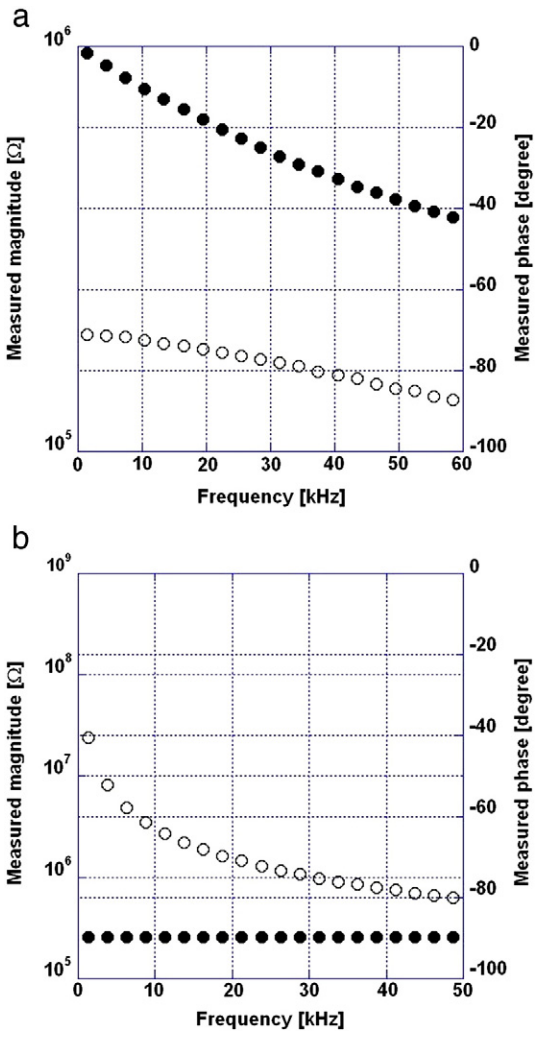

Fig. 5. Impedance measurement of a) a 205 μm × 30 μm $SrRuO_3$(100 nm)/$LaYbO_3$(300 nm)/$SrRuO_3$(150 nm) parallel plate capacitor when the $LaYbO_3$ grown at a pressure of 40 Pa. (b) A 205 μm × 30 μm $SrRuO_3$(100 nm)/$LaYbO_3$(580 nm)/$SrRuO_3$(150 nm) parallel plate capacitor when the $LaYbO_3$ was grown at a 0.40 Pa of O_2. The open circles (○) show the magnitude of the impedance, while the full circles (●) show the phase angle.

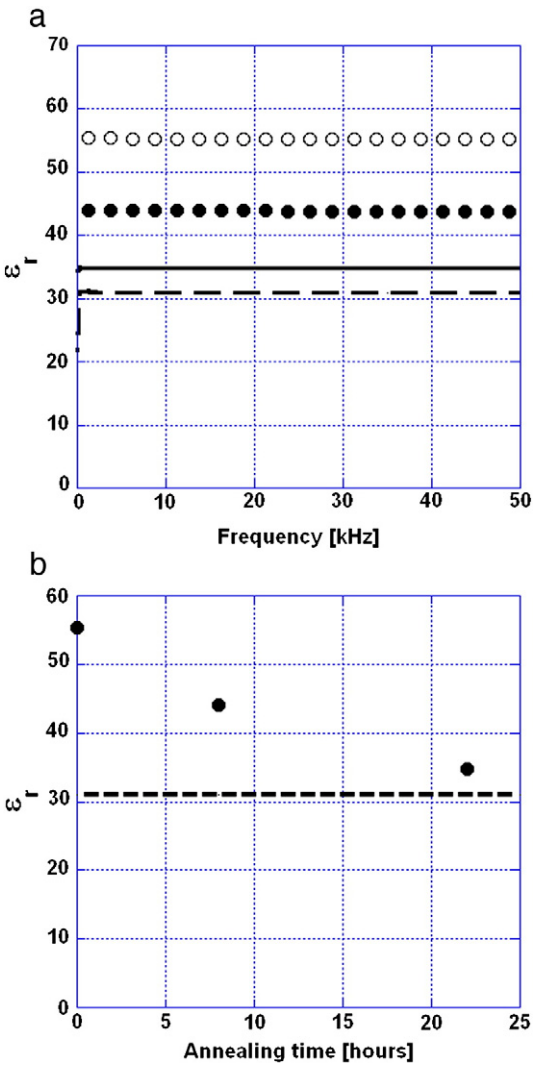

Fig. 6. a) Relative permittivity as a function of frequency for $SrRuO_3/LaYbO_3/SrRuO_3$ parallel plate capacitors. The open circles (○) show the relative permittivity of a capacitor fabricated by the first method as grown; the full circles (●) and the dashed line (– –) show the lowered values of relative permittivity after annealing at 500 °C in $100*10^5$ Pa oxygen for 8 h and 22 h respectively. The capacitor has an area of 6150 μm^2 and a $LaYbO_3$ layer is 583 nm thick. The continuous line (–) shows the dielectric constant of a second capacitor where the $SrRuO_3/LaYbO_3/SrRuO_3$ stack was grown in situ by the second method, and not annealed. This second device has an area of 49,350 μm^2 and a $LaYbO_3$ layer which is 567 nm thick. For both samples the $SrRuO_3$ bottom and top electrode layers are 150 nm and 100 nm thick respectively. b) Relative permittivity as a function of annealing time for $SrRuO_3/LaYbO_3/SrRuO_3$ parallel plate capacitors. The open full circles (●) show the relative permittivity of a capacitor fabricated by the first method as a function of the annealing time; the annealing was performed at 500 °C in 10^5 Pa oxygen. The capacitor has an area of 6150 μm^2 and the $LaYbO_3$ layer is 583 nm thick. The dashed line (– –) shows the dielectric constant of a second capacitor where the $SrRuO_3/LaYbO_3/SrRuO_3$ stack was grown in situ by the second method, and not annealed. This second device has an area of 49,350 μm^2 and a $LaYbO_3$ layer which is 567 nm thick. For both samples the $SrRuO_3$ bottom and top electrode layers are 150 nm and 100 nm thick respectively.

3.2. Impedance measurements

Impedance measurements of the $SrRuO_3/LaYbO_3/SrRuO_3$ trilayers showed that when the $LaYbO_3$ was grown in flowing oxygen at a pressure of 40 Pa the capacitive structures presented resistive losses. This can be seen from the phase angle of the impedance in Fig. 5a. The phase angle is close to zero at low frequency, indicating conducting behavior, and becomes more negative as the frequency increases, indicating lossy capacitive behavior at high frequencies. Near-ideal capacitive behavior was found for $LaYbO_3$ films grown in oxygen at a pressure of 0.40 Pa, as shown by the phase angle of −90° in Fig. 5b. The data shown in Fig. 5 correspond to capacitors prepared by the first method although the better properties for lower pressure deposition were found in both preparation methods.

A similar decrease in dielectric losses with decreased deposition pressure was reported for $SrRuO_3/BaTiO_3/SrRuO_3$ capacitive structures also grown by PLD [8]. During PLD, depending on the surface mobility of the adatoms, the growth of the film may be accompanied by the formation of stacking faults and amorphous and void-like grain boundaries [12]. The surface mobility of the adatoms is influenced by the deposition pressure, the substrate temperature and the laser energy. High deposition pressures imply a large number of collisions in the path between the target and the substrate. The kinetic energy lost in the path produces a lower mobility of the atomic species on the substrate [13].

Impedance measurements on $SrRuO_3/LaYbO_3/SrRuO_3$ capacitors allow the calculation of the permittivity of the $LaYbO_3$ by using the expression for the impedance of the capacitor [14]:

$$z(j\omega) = \frac{1}{j\omega C}. \tag{2}$$

In Eq. (2), ω is the angular frequency, C is the capacitance and j is the imaginary number.

Eq. (2) is valid for a capacitor with no resistive losses, as indicated by the impedance phase angle of −90° throughout the frequency range for the capacitors grown at 0.40 Pa.

The capacitance of a parallel plate capacitor is given by [14]:

$$C = \frac{\varepsilon_0 \varepsilon_r A}{d}. \quad (3)$$

In Eq. (3), ε_0 is the permittivity of the vacuum, ε_r is the relative permittivity of the dielectric layer, A is the area of the capacitor and d is the distance between the two electrodes.

The relative permittivities deduced from the magnitude of the impedances for all samples are higher than the value of 26 for bulk materials [4]. A similar behavior was reported for $SrRuO_3/LaLuO_3/SrRuO_3$ and $YBa_2Cu_3O_7/SrTiO_3/YBa_2Cu_3O_7$ capacitors prepared by PLD [5,15]. Figs. 6a and 6b show the relative permittivity of two devices, one built with the first fabrication process (i.e. with the patterning of the bottom electrode before completion of the tri-layer sequence) and the other built with the second fabrication process (i.e. all the patterning performed after deposition of the tri-layer). In both cases the $LaYbO_3$ was grown in the lower oxygen pressure of 0.40 Pa. The critical difference between the two samples is the presence of damage on the bottom electrode due to patterning in the sample grown by the first method.

The open circles (○) in Fig. 6a represent the relative permittivity of the $LaYbO_3$ layer belonging to a capacitive structure fabricated with the first process. The measured value is approximately twice the value measured in bulk material. An enhanced permittivity was also found in $YBa_2Cu_3O_7/SrTiO_3/YBa_2Cu_3O_7$ capacitive structures grown by PLD in which the $YBa_2Cu_3O_7$ bottom electrode was patterned by standard photolithography and argon ion-beam milling [15]. This behavior was attributed to the presence of defects and to the island growth of the $SrTiO_3$ which led to space charge polarization in the dielectric layer. As already discussed in Section 3.1 the edges of the $SrRuO_3$ bottom electrode of the sample fabricated by the first procedure are expected to be damaged by argon ion bombardment. The damaged areas do not constitute a good seed layer for the growth of the $LaYbO_3$. These regions might not have the right stoichiometry or may present a higher density of defects and stacking faults, leading to space charge polarization in the $LaYbO_3$ film and an increased permittivity. After 8 h of annealing the relative permittivity at room temperature was reduced to 44 as shown in Fig. 6a and in Fig. 6b. After 22 h of annealing its value was around 31 as shown in Fig. 6a and 6b. The reduction in relative permittivity is most likely connected to the improvement in crystallinity discussed in Section 3.1. Changes in strain, both homogeneous and heterogeneous, have been shown to influence dielectric properties significantly [16].

When the samples were grown by the second method, in one step and completely in-situ, the relative permittivity of the $LaYbO_3$ film was 36, as shown by the solid line in Fig. 6a, about 35% higher than that measured in bulk material.

Both preparation routes yielded values of relative permittivity higher than the relative permittivity of the bulk material. These higher values might be attributed to a higher permittivity along the $LaYbO_3$ $(001)_o$ axis as Schubert et al. [5] suggested in the case of $LaLuO_3$ films.

4. Conclusions

The crystal structures and the dielectric properties of $SrRuO_3/LaYbO_3/SrRuO_3$ capacitive structures were investigated and assessed. When the capacitive structures were fabricated with the patterning of the bottom electrode layer before deposition of the $LaYbO_3$ film, misoriented regions were present in the $LaYbO_3$ film and the relative permittivity was twice that of bulk $LaYbO_3$. The high value is attributed to the presence of defects between the edge of the bottom electrode and the $LaYbO_3$ film which leads to a space charge polarization in the $LaYbO_3$ layer [5,15].

Post-growth annealing recrystallized the damaged regions in the $SrRuO_3$ and the $LaYbO_3$ and the permittivity was lowered towards the bulk value. When the $SrRuO_3/LaYbO_3/SrRuO_3$ stack was grown in one step, the relative permittivity of the $LaYbO_3$ was comparable with that of the annealed film grown by the two-step method. In both cases the values of the relative permittivity were still higher than that of bulk $LaYbO_3$. This is attributed to anisotropy of the relative permittivity, with the highest values along the (00*l*) axis [5].

Acknowledgments

The Panalytical diffractometer used in this research was obtained through Birmingham Science City Project: Creating and Characterizing Next Generation Advanced Materials with support from Advantage West Midlands and part-funded by the European Regional Development Fund. The film growth and impedance measurements were funded by the University of Birmingham.

References

[1] D.H. Triyoso, D.C. Gilmer, J. Jiang, R. Droopad, Microelectron. Eng. 85 (2008) 1732.
[2] J.M.J. Lopes, M. Roeckerath, T. Heeg, U. Littmark, J. Schubert, S. Mand, Y. Jia, D.G. Schlom, Microelectron. Eng. 84 (2007) 1890.
[3] J. Varghese, T. Joseph, M.T. Sebastian, N. Reeves-McLaren, A. Feteira, J. Am. Ceram. Soc. 93 (2010) 2960.
[4] A. Feteira, L.J. Gillie, R. Elsebrock, D.C. Sinclair, J. Am. Ceram. Soc. 90 (2007) 1475.
[5] J. Schubert, O. Trithaveesak, W. Zander, M. Roeckerath, T. Heeg, H.Y. Chen, C.L. Jia, P. Meuffels, Y. Jia, D.G. Schlom, Appl. Phys. A: Mater. 90 (2008) 577.
[6] H.J.H. Smilde, H. Hilgenkamp, G.J. Gerritsma, D.H.A. Blank, H. Rogalla, IEEE Trans. Appl. Supercond. 11 (2001) 501.
[7] F.X. Wang, W. Li, F. Lu, H. Hu, K.M. Wang, Z.G. Liu, Y. Zhu, Nucl. Instrum. Methods Phys. Res. B 191 (2002) 778.
[8] G. Vasta, T.J. Jackson, E. Tarte, Thin Solid Films 520 (2012) 3071.
[9] C. Aruta, M. Angeloni, G. Balestrino, P.G. Medaglia, P. Orgiani, A. Tebano, J. Zegenhagen, Eur. Phys. J. B 46 (2005) 251.
[10] P. Orgiani, C. Aruta, G. Balestrino, S. Lavanga, P.G. Megaglia, A. Tebano, Eur. Phys. J. B 26 (2002) 23.
[11] D.E. Daush, G.H. Haertling, in: Application of Ferroelectrics, 1992, p. 297.
[12] D. Su, T. Yamada, R. Gysel, A.K. Tagantsev, P. Murat, N. Setter, N. Jiang, J. Mater. Res. 26 (2011) 770.
[13] S. Proyer, E. Stangl, M. Borz, B. Hellebrand, D. Bauerle, Physica C 257 (1996) 1.
[14] E. Hughes, J. Hiley, K. Brown, I. McKenzie Smith, Electrical and Electronic Technology, Pearson, Harlow, 2012.
[15] B. Prijamboedi, H. Takashima, R. Wang, A. Shoji, M. Itoh, J. Alloys Compd. 449 (2008) 48.
[16] Y.Y. Tse, P.M. Suherman, T.J. Jackson, I.P. Jones, Philos. Mag. 88 (2008) 2505.